

# Fine-Grained Image-Text Alignment in Medical Imaging Enables Cyclic Image-Report Generation

Wenting Chen<sup>1</sup>, Xiang Li<sup>2</sup>, Linlin Shen<sup>3</sup> and Yixuan Yuan<sup>4\*</sup>

<sup>1</sup>City University of Hong Kong <sup>2</sup>Massachusetts General Hospital and Harvard Medical School

<sup>3</sup>Shenzhen University <sup>4</sup>The Chinese University of Hong Kong

## Abstract

*Fine-grained vision-language models (VLM) have been widely used for inter-modality local alignment between the predefined fixed patches and textual words. However, in the medical analysis, lesions exhibit varying sizes and positions, and the fixed patches may cause incomplete representations of lesions. Moreover, these methods provide explainability by using heatmaps to show the general potential image areas associated with texts rather than specific regions, making their explanations not explicit and specific enough. To address these issues, we propose a novel Adaptive patch-word Matching (AdaMatch) model to correlate chest X-ray (CXR) image regions with words in medical reports and apply it to CXR-report generation to provide explainability for the generation process. AdaMatch exploits the fine-grained relation between adaptive patches and words to provide explanations of specific image regions with corresponding words. To capture the abnormal regions of varying sizes and positions, we introduce the Adaptive Patch extraction (AdaPatch) module to acquire the adaptive patches for these regions adaptively. In order to provide explicit explainability for CXR-report generation task, we propose an AdaMatch-based bidirectional large language model for Cyclic CXR-report generation (AdaMatch-Cyclic). It employs the AdaMatch to obtain the keywords for CXR images and ‘keypatches’ for medical reports as hints to guide CXR-report generation. Extensive experiments on two publicly available CXR datasets prove the effectiveness of our method and its superior performance to existing methods.*

## 1. Introduction

Inter-modality alignment, such as vision and language, has been an important task with growing interests in the field of computer vision, especially with the recent advancement in representation learning [34]. Technologies like con-

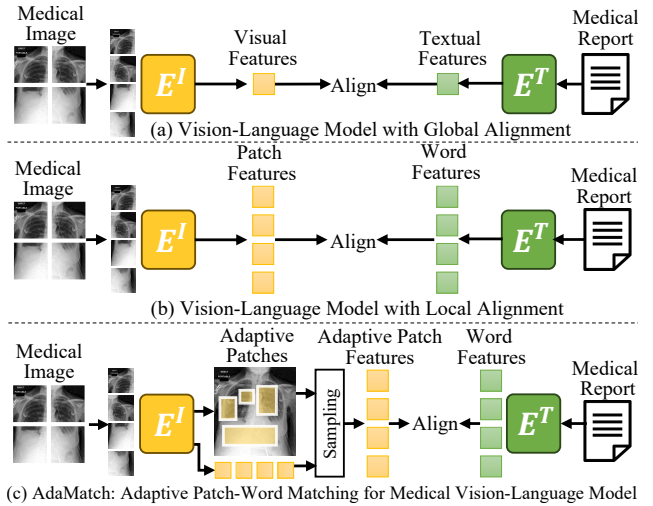


Figure 1. Current vision-language models (VLM) achieve (a) global alignment and (b) local alignment by matching overall visual with textual features, and aligning patch with word features, respectively. (c) To exploit the relation between textual words and abnormal patches with different sizes, the proposed AdaMatch obtains adaptive patch features and aligns them with word features.

trastive learning and self-supervised learning have dramatically improved state-of-the-art alignment performance. Recent vision-language models (VLMs) demonstrate two approaches: global contrastive alignment, which integrates images and texts at a global level [17, 19, 34, 44, 46], and local alignment, focusing on detailed connections between visual objects and textual words [6, 21, 24, 25, 50, 52], as illustrated in Fig. 1.

Current VLMs with local alignment either adopt the pre-trained object detector to extract region-of-interest (ROI) features from images and match the corresponding object features with textual words [6, 24, 25, 52]; or align the visual token from each patch and the textual token into the same embedding space [18, 21, 41, 50]. The former highly relies on the quality of the object detector and its

\*Corresponding authors: Yixuan Yuan (yxyuan@ee.cuhk.edu.hk)

predefined classes, which is less generalizable to new domains. The latter family of methods learns the alignment in a more automatic and data-driven manner. However, most of these methods depend on pre-defined patch size and position (e.g., grids) across images. In most challenging cases, such as the analysis of medical image analysis, lesions can exhibit a wide range of shapes, sizes, and positions. A fixed definition of image patches can lead to incomplete or ambiguous representations of the key imaging abnormalities. Hence, it is highly needed to adaptively exploit the fine-grained relationship between image embeddings derived from a more flexible patching scheme and textual embeddings.

Another challenge in the current local medical VLMs lies in their explainability: it is generally difficult to delineate the image-text relationship learned by the model, especially for the current medical VLMs. Current solutions to provide such explanations in medical VLMs leverage the attention maps from the intermediate layer to visualize the location of the abnormalities [16, 32, 45]. Other methods [5, 28, 40] utilize network gradients such as Grad-CAM [38] to generate the heatmaps according to lesion types based on ground-truth reports. However, both maps can only show the general potential areas associated with the corresponding text data rather than clearly pinpointing a specific region. In addition, gradient-based methods need ground-truth reports, prohibiting them from functioning correctly beyond training data. It is thus highly necessary to develop a mechanism that could provide explicit and specific explanations of the input image or text during inference time.

To address these two challenges above, we propose a novel Adaptive patch-word Matching (AdaMatch) model to match fine-grained image regions of various sizes and positions with textual data. AdaMatch introduces an image encoder with multiple Adaptive Patch extraction (AdaPatch) modules to adaptively acquire the patches associated with certain text tokens. It then performs patch-word alignment based on contrastive learning. AdaMatch is specifically developed in the context of aligning radiology images (chest X-ray, CXR) and their corresponding radiology reports with the capability of achieving cyclic (CXR-to-report and report-to-CXR) generation based on the learned alignment. Our premise is that such a cyclic generation task would serve as the best use case and evaluation criterion for the desired fine-grained alignment. Also, the fine-grained cyclic generation between CXR and report will provide a natural explainability for how the model aligns the two modalities: for any given text token, we can visualize its matching imaging manifestation; and for any image region within a CXR image, we can tell the type of lesion or anatomical region it belongs to.

To implement the cyclic CXR-report generation, we pro-

pose an AdaMatch-based bidirectional model (AdaMatch-Cyclic). AdaMatch-Cyclic employs AdaMatch to identify the keywords for CXR images and ‘keypatches’ for medical reports to guide the generation tasks. Since the potential keywords for CXR images cover a wide range and ground-truth reports cannot be used during inference, we predefine a textual codebook with the most common entities from medical reports as prior knowledge during fine-grained alignment. With the textual codebook, AdaMatch aligns it with the adaptive patches to obtain matched keywords as guidance for report generation. Next, a VQ-GAN model encodes the CXR image into image tokens, and a Large Language Model (LLM) takes image tokens, the matched keywords, and the instructions as input to generate the medical reports. Similarly, we also build a visual codebook with the most commonly seen patches as ‘keypatches’, and use AdaMatch to obtain the matched keypatches from given text reports as hints for CXR generation. With medical reports, matched keypatches, and instructions, LLM outputs the image tokens, and then the VQ-GAN model decodes them into the generated CXR image. Our contributions are summarized as follows:

- To exploit the fine-grained relation between the CXR image patches with words of medical reports, we propose an Adaptive patch-word Matching (AdaMatch) model to obtain adaptive patches for abnormal regions and perform alignment between them and texts in medical reports.
- We devise an AdaMatch-based bidirectional LLM for Cyclic CXR-report generation (AdaMatch-Cyclic) to facilitate the generation between CXR and reports. Moreover, we build the textual and visual codebook to utilize AdaMatch to extract useful keywords and keypatches for the report and CXR generation, respectively.
- Experiments on two publicly available chest X-ray datasets demonstrate the effectiveness of our method and its superior performance over state-of-art methods.

## 2. Related Works

### 2.1. Fine-Grained Vision-Language Models

Recently, several fine-grained vision-language models (VLM) [6, 18, 21, 24, 25, 41, 50, 52] achieve the local alignment by exploiting the fine-grained relation between visual objects and textual words. Some methods [6, 24, 25, 52] employ the pre-trained object detector to obtain region-of-interest (ROI) features from images and align the object features with textual features, and others [18, 21, 41, 50] aim to locally align the fixed patches with the textual words. For instance, Li *et al.* [24] utilizes Faster-RCNN [36] to detect visual objects and match ROI embeddings with textual embeddings. Moreover, FILIP [50] achieves cross-modal interaction by maximizing the similarity between the visual tokens of fixed patches and textual tokens. The former

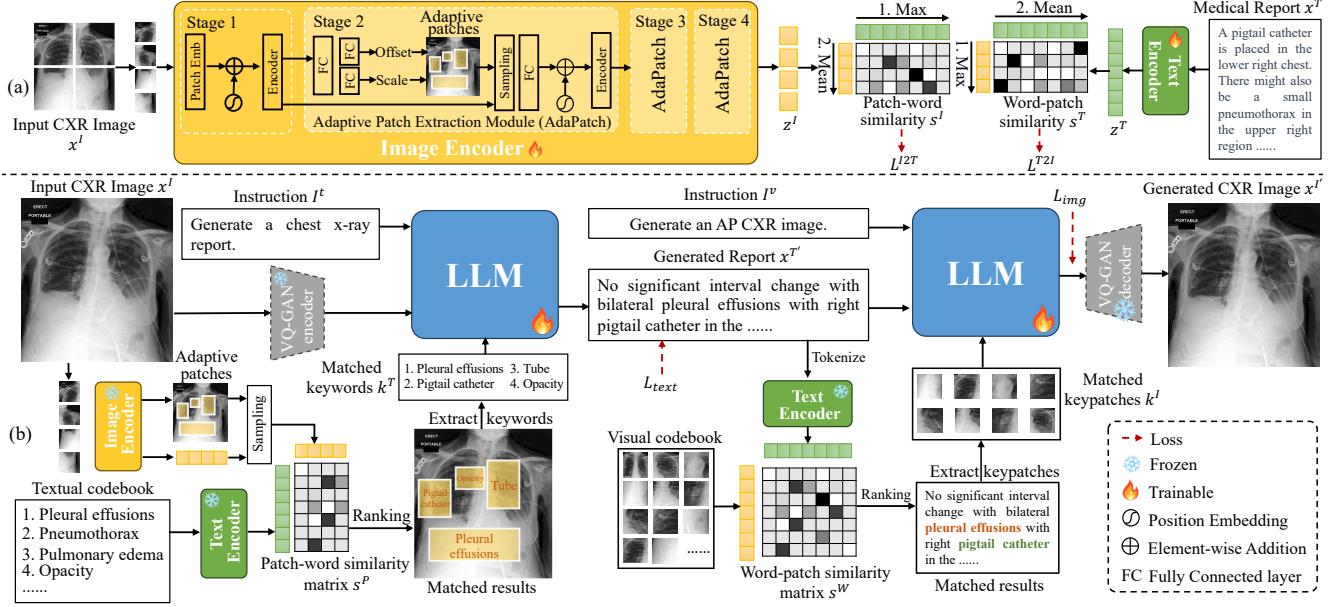


Figure 2. The overview of the proposed methods. (a) Adaptive patch-word Matching (AdaMatch) model. (b) AdaMatch-based bidirectional large language model (LLM) for cyclic CXR-report generation (AdaMatch-Cyclic).

requires a precise object detector, and the latter primarily learns the relation between fixed patches inside the predefined grid and words. Nevertheless, when lung lesions differ in size, shape, and position, these methods may split them into separate patches, leading to incomplete semantic information of patches. Thus, we devise an Adaptive patch-word Matching (AdaMatch) model to adaptively exploit the fine-grained relation between flexible patches and textual words.

## 2.2. CXR-Report Generation

Medical VLMs are widely used in downstream tasks for chest radiographs, including CXR-to-report generation [7, 8, 39, 42, 47, 48] and report-to-CXR generation [2, 3, 22, 23, 37] tasks. CXR-to-report generation has been investigated to reduce the burden of radiologists and promote clinical automation. For instance, Chen *et al.* [8] introduces a cross-modal memory network with shared memory to align images with texts to promote report generation performance. In report-to-CXR generation task, previous methods generate high-quality and annotated CXR images from medical reports, to provide more training data and avoid privacy laws and considerations. Some diffusion-based methods [2, 22] take the impression section of reports as input, ignoring the finding section that includes detailed descriptions. To consider more details in reports, several transformer-based methods [22, 23] take both finding and impression sections as input to synthesize CXR. In this paper, we use the cyclic generation (i.e. CXR-to-report and report-to-CXR generation) as use case and evaluation criteria for our fine-grained alignment method (AdaMatch). We

also design an AdaMatch-Cyclic to employ AdaMatch to improve the explainability of cyclic generation.

## 3. Methods

In Fig. 2, we propose an adaptive patch-word matching (AdaMatch) model to associate the CXR image regions with words in medical reports, and apply it to CXR-report generation to provide explainability. Given an input CXR image  $x^I$ , the image encoder with several Adaptive Patch extraction modules (AdaPatch) predicts the location and scale of multiple adaptive patches and processes the adaptive patch embeddings  $z^I$ . With  $z^I$  and text embeddings  $z^T$  extracted by text encoder for the medical report  $x^T$ , we compute the similarities  $s^I$ ,  $s^T$  between adaptive patches and text tokens to calculate the contrastive loss  $L_{I2T}$ ,  $L_{T2I}$  to optimize AdaMatch model. For CXR-to-report generation, we utilize the frozen AdaMatch model to match a predefined textual codebook with the input CXR image  $x^I$  to obtain matched keywords  $k^T$  and feed a LLM with  $k^T$ , the instruction, and image tokens encoded by VQ-GAN from  $x^I$  to generate a medical report  $x^{T'}$ . Then, the AdaMatch model is used to match a predefined visual codebook with the generated report  $x^{T'}$  to acquire the matched keypatches  $k^I$ . With instruction,  $x^{T'}$  and  $k^I$ , LLM outputs image tokens of the generated CXR image  $x^{I'}$ , which is optimized by  $L_{text}$  and  $L_{img}$ .

### 3.1. Adaptive Patch-Word Matching (AdaMatch)

Current VLMs [6, 21, 24, 25, 50, 52] achieve fine-grained alignment between visual objects and textual words, but they may split lung lesions into separate fixed patches due to various shapes, sizes, and positions of lung lesions. Thus, we propose an Adaptive patch-word Matching (AdaMatch) to automatically locate the important regions, extract adaptive patches for these regions, and align them with corresponding textual words. As shown in Fig. 2 (a), AdaMatch includes an image encoder to extract adaptive patch features and a text encoder to encode textual features.

**Image Encoder.** To obtain the adaptive patches, the image encoder consists of four stages with feature maps of decreasing scales. Specifically, in the first stage, we first adopt the patch embedding module to split the CXR image  $x^I \in \mathbb{R}^{H \times W \times C}$  into  $N$  patches with fixed size  $s \times s$  and project them to patch embeddings  $z^{(i)} (1 \leq i \leq N)$  through a fully connected layer  $g$ ,  $z^{(i)} = g([a^{(i,1)}; \dots; a^{(i,s \times s)}])$ , where  $a^{(i,j)}$  indicates the image features for the pixel located at  $q^{(i,j)}$  and  $[\cdot]$  denotes the concatenation operation. Afterward, we pass the patch embeddings  $z^{(i)}$  with the position embeddings  $e_{pos}$  into a transformer encoder [43]  $R$  to obtain the outputs,  $z^{(i)} = R(z^{(i)} + e_{pos})$ , where  $R$  includes an attention layer and a feed-forward layer. In order to locate the potential lung lesions, we devise an **Adaptive Patch Extraction module (AdaPatch)** for the rest of stages. In AdaPatch, a fully connected layer is fed with patch embeddings  $z^{(i)}$ , and then the outputs are passed through four separate fully connected layers  $f_1, f_2, f_3, f_4$  to predict the offset  $(\delta_x^{(i)}, \delta_y^{(i)})$  and patch size  $(s_w^{(i)}, s_h^{(i)})$  for the adaptive patches, where the offset indicates the shift to the center of original fixed patches  $(c_x^{(i)}, c_y^{(i)})$ ,

$$\delta_x^{(i)} = \text{Tanh}(f_1(z^{(i)})), \delta_y^{(i)} = \text{Tanh}(f_2(z^{(i)})), \quad (1)$$

$$s_w^{(i)} = \text{ReLU}(\text{Tanh}(f_3(z^{(i)}))), s_h^{(i)} = \text{ReLU}(\text{Tanh}(f_4(z^{(i)}))). \quad (2)$$

With the offset and patch size, we compute the position of left-top  $(a_x^{(i)}, a_y^{(i)})$  and right-bottom corners  $(b_x^{(i)}, b_y^{(i)})$  for each adaptive patch,

$$a_x^{(i)} = c_x^{(i)} + \delta_x^{(i)} - \frac{s_w^{(i)}}{2}, a_y^{(i)} = c_y^{(i)} + \delta_y^{(i)} - \frac{s_h^{(i)}}{2}, \quad (3)$$

$$b_x^{(i)} = c_x^{(i)} + \delta_x^{(i)} + \frac{s_w^{(i)}}{2}, b_y^{(i)} = c_y^{(i)} + \delta_y^{(i)} + \frac{s_h^{(i)}}{2}, \quad (4)$$

and uniformly sample  $m \times m$  feature points inside the patches. Since the coordinates may be fractional, bilinear interpolation is used to obtain the sampled feature points  $\{\hat{p}^{(j)}\}_{1 \leq j \leq m \times m}$ . The embeddings of all sampled points are flattened and fed into a fully connected layer  $f_5$  to obtain patch embeddings,  $z^{(i)} = f_5([\hat{p}^{(i,1)}; \dots; \hat{p}^{(i,m \times m)}])$ . Finally, we pass  $z^{(i)}$  with position embeddings  $e_{pos}$  into a

transformer encoder  $R$ . The final adaptive patch embeddings  $z^I \in \mathbb{R}^{N \times d}$  are the ensemble of  $z^{(i)} (1 \leq i \leq N)$ ,  $z^I = E^I(x^I) = \{z_1^I, \dots, z_N^I\}$ , where  $E^I$ ,  $x^I$ , and  $d$  denote the image encoder, the input CXR image, and the dimension of adaptive patch embeddings, respectively.

**Text Encoder.** We adopt the BioClinicalBERT [1] as the text encoder  $E^T$  to encode the medical report  $x^T$  into text embeddings  $z^T$ . To make  $z^T$  with the same dimension as  $z^I$ , we feed a fully connected layer with  $z^T$  to reduce its dimension,  $z^T = E^T(x^T) = \{z_1^T, \dots, z_K^T\} (z^T \in \mathbb{R}^{K \times d})$ , where  $K$  denotes the number of text tokens.

**Patch-Word Alignment.** In order to exploit the relation between the adaptive patches and textual tokens, we perform fine-grained contrastive representation learning to achieve patch-word alignment. Concretely, for the  $i$ -th CXR image  $x_i^I$  and  $j$ -th medical report  $x_j^T$ , we first compute the similarities between all the adaptive patch embeddings  $z_n^I (1 \leq n \leq N)$  and all the text embeddings  $z_k^T (1 \leq k \leq K)$ , and use the largest similarity  $\max_{(1 \leq k \leq K)} (z_n^I)^\top z_k^T$  as the patch-word maximum similarity for  $n$ -th adaptive patch embedding. Then, the patch-word maximum similarities for all the adaptive patch embeddings are averaged as the similarity  $s_{i,j}^I$  of the  $i$ -th CXR image to the  $j$ -th medical report,

$$s_{i,j}^I = \frac{1}{N} \sum_{n=1}^N (z_n^I)^\top z_{m_n^I}^T, \quad (5)$$

where  $m_n^I = \arg \max_{(1 \leq k \leq K)} (z_n^I)^\top z_k^T$ . Similarly, the similarity of the  $j$ -th medical report to the  $i$ -th CXR image is defined as,

$$s_{i,j}^T = \frac{1}{K} \sum_{k=1}^K (z_{m_k^T}^I)^\top z_k^T, \quad (6)$$

where  $m_k^T = \arg \max_{(1 \leq n \leq N)} (z_n^I)^\top z_k^T$ . We exclude the padded textual tokens when computing the similarity.

With the cross-modal similarities  $s_{i,j}^I$  and  $s_{i,j}^T$  for the  $i$ -th CXR image and  $j$ -th medical report, we compute the adaptive patch-word contrastive loss  $L_i^I$  for  $i$ -th CXR image  $x_i^I$ ,

$$L_i^{I2T}(x_i^I, \{x_j^T\}_{j=1}^b) = -\frac{1}{b} \log \frac{\exp(s_{i,i}^I/\tau)}{\sum_j \exp(s_{i,j}^I/\tau)}, \quad (7)$$

where  $b$  denotes the batch size,  $\tau$  represents temperature hyperparameter and  $\{x_i^I, x_i^T\}$  indicates the positive CXR-report pair. Similarly, the adaptive word-patch contrastive loss  $L_i^T$  for  $i$ -th medical report  $x_i^T$  is formulated as,

$$L_i^{T2I}(x_i^T, \{x_j^I\}_{j=1}^b) = -\frac{1}{b} \log \frac{\exp(s_{i,i}^T/\tau)}{\sum_j \exp(s_{j,i}^T/\tau)}. \quad (8)$$

The final contrastive loss for a mini-batch is calculated by,

$$L = \frac{1}{2} \sum_{i=1}^b (L_i^{I2T} + L_i^{T2I}). \quad (9)$$



```

Below is an instruction that describes a task,
paired with an input that provides further
context. Write a response that appropriately
completes the request.
### Instruction: Utilize the entered chest X-ray
images to generate comprehensive free-text
radiology reports.
### Input: 66, 260, 379, 555, 304, ..., 905
### Keywords: Pleural effusions, tube
### Response: A pigtail catheter is placed in the
lower right chest .....

```

Figure 3. Instruction data example for CXR-to-report generation.

```

Below is an instruction that describes a task,
paired with an input that provides further
context. Write a response that appropriately
completes the request.
### Instruction: Create an AP chest X-
ray image that matches the free-
text radiology reports.
### Input: A pigtail catheter is placed in
the lower right chest .....
### Keypatches: 122, 680, 978
### Response: 719, 421, 551, 421, 742,..., 905

```

Figure 4. Instruction data example for report-to-CXR generation.

With the final contrastive loss, the image and text encoders are optimized to automatically locate the important patches with varied sizes and exploit the fine-grained relation between the patches and words.

### 3.2. AdaMatch-based LLM for Cyclic CXR-Report Generation (AdaMatch-Cyclic)

To provide explicit explainability for CXR-report generation task, we propose an AdaMatch-based bidirectional LLM for the cyclic CXR-report generation (AdaMatch-Cyclic) by locating the potential lesions in CXR images and visualizing the appearance of description in reports to guide the generation process, as depicted in Fig. 2 (b).

#### 3.2.1 CXR-to-Report Generation

In CXR-to-report generation, we employ the AdaMatch to match a predefined textual codebook with the CXR image to obtain the matched keywords as hints to guide LLM to generate reports.

**Building textual codebook.** Specifically, to establish a textual codebook, we use a pre-trained BioEN [35] to extract the related entities from the medical reports in the training set, where the related entities are divided into four entity groups, i.e., biological structure, detailed description, disease disorder, and sign symptom. Next, we compute the frequency of each entity and pick top  $\kappa_0$  entities for each entity group as keywords in the textual codebook.

**Keywords Extraction.** With the textual codebook, we employ the frozen AdaMatch model to match the keywords from the textual codebook with the adaptive patches of CXR images, and obtain a patch-word similarity matrix  $s^P \in \mathbb{R}^{M \times N}$  between the keyword tokens and adaptive patch embeddings, where  $M$  and  $N$  denote the number of keyword tokens and adaptive patches. To extract the most matched keywords for each adaptive patch, we rank the patch-word similarity along the dimension of keyword tokens, obtain the top  $\kappa_1$  patch-word similarities for each adaptive patch, and extract the corresponding keywords  $k^T$ . The matched keywords can explain potential lesions in each adaptive patch, to assist LLM in generating medical reports.

**Instruction tuning LLM.** After keywords extraction, we use a frozen VQ-GAN [13] encoder  $E$  to encode the input CXR image  $x^I$  to the quantized image latent vectors as image tokens  $E(x^I)$ . For CXR-to-report generation, the dolly-v2-3b [9] model is adopted as the bidirectional LLM, which is pre-trained on the instruction-following dataset. When fine-tuning LLM, we convert CXR-to-report generation dataset in instruction-following format. An example of instruction data for CXR-to-report generation is shown in Fig. 3, including the instruction, input, keywords, and response parts, where input is the image tokens of the input CXR image, keywords are extracted by AdaMatch, and response is the ground-truth medical report. During training, the response part is hidden and the LLM learns to generate it in autoregressive manner.

By adopting AdaMatch-Cyclic for CXR-to-report generation, we can locate the potential lesion in CXR images, to provide more explainability for the generation process.

#### 3.2.2 Report-to-CXR Generation

In report-to-CXR generation, we leverage the AdaMatch to match a predefined visual codebook with the generated reports  $x^T$  to acquire matched keypoints as guidance for LLM to synthesize CXR images, where ‘keypatches’ are important image patches related to generated reports.

**Building visual codebook.** Concretely, we first construct a visual codebook with the most common adaptive patches as keypoints. To collect the most common adaptive patches for CXR images in the training set, the AdaMatch is utilized to match the adaptive patches of CXR images with textual tokens of medical reports to obtain top  $\kappa_2$  CXR-report pairs with the highest report-to-CXR similarities  $s^T$ . For each CXR-report pair, we compute the word-patch maximum similarity  $\max_{(1 \leq n \leq N)} (z_n^I)^\top z_k^T$  for each textual token, rank the word-patch maximum similarities, and extract the adaptive patches for top  $\kappa_3$  similarities as keypoints in the visual codebook. Each keypatch includes its adaptive patches and the corresponding features.

**Keypatches Extraction.** With the visual codebook, the frozen AdaMatch matches the features of keypoints in

the visual codebook with textual tokens of the generated report to acquire the word-patch similarity matrix  $s^W \in \mathbb{R}^{(\kappa_2 \times \kappa_3) \times K}$ , where  $K$  denotes the number of textual tokens for the generated report. To obtain keypatches related to the generated report, we rank the word-patch similarity along the dimension of keypatches, obtain the top  $\kappa_4$  word-patch similarity for each textual token, and extract the features of corresponding keypatches  $k^I$ .

**Instruction tuning LLM.** After keypatches extraction, we employ a frozen VQ-GAN encoder to convert the matched keypatches  $k^I$  into image tokens  $E(k^I)$ , and feed the pre-trained LLM with the instruction, the generated report, and image tokens of keypatches in the instruction-following format, as shown in Fig. 4. Then, LLM predicts the image tokens and the VQ-GAN decoder decodes the image tokens into the corresponding generated CXR image  $x^{I'}$ .

AdaMatch-Cyclic allows us to interpret generated reports with matched keypatches, thereby providing explainability to the generation procedure.

### 3.2.3 Overall Objective

To optimize AdaMatch-Cyclic, we apply the standard language modeling objective for both CXR-to-report and report-to-CXR generation. For CXR-to-report generation, LLM is fed with the instruction  $I^t$ , image tokens of input CXR image  $E(x^I)$ , and matched keywords  $k^T$  in instruction-following format, and LLM aims to generate the ground-truth medical report of response part autoregressively. We compute the  $P(u_k)$  conditional probability of the  $k$ -th token,  $P(u_k) = \mathcal{LLM}(I^t, E(x^I), k^T)$ , where  $k$  is the token index after the response key (### Response:). The report generation loss  $L_{text}$  for the response area is calculated by,

$$L_{text} = \sum_{i=k}^n -\log P(u_i | u_1, u_2, \dots, u_{i-1}), \quad (10)$$

where  $[u_1, u_2, \dots, u_{i-1}]$  denotes the tokenized texts before the response part, and  $n$  represents the maximum length of output tokens.

Similarly, for report-to-CXR generation, we feed the LLM with the instruction  $I^v$ , the generated report  $x^{T'}$ , and the image tokens of keypatches  $E(k^I)$  in the instruction-following format, and obtain the conditional probability of  $k$ -th token  $w_k$ ,  $P(w_k) = \mathcal{LLM}(I^v, x^{T'}, E(k^I))$ . The CXR generation loss  $L_{img}$  is defined as:

$$L_{img} = \sum_{i=k}^n -\log P(w_i | w_1, w_2, \dots, w_{i-1}), \quad (11)$$

With  $L_{text}$  and  $L_{img}$ , the LLM can implement the bidirectional CXR and report generation according to instructions.

## 4. Experiments

### 4.1. Experiment Setting

**Datasets.** We conduct our experiments on two main publicly available chest X-ray datasets, i.e. MIMIC-CXR [20] and OpenI [11] datasets. **MIMIC-CXR** dataset is the largest public dataset for chest radiographs, including 473,057 chest X-ray images and 206,563 reports from 63,478 patients. We follow the official splits, i.e. 368,960 instances for training, 2,991 for validation, and 5,159 for testing. **OpenI** is a chest X-ray dataset with 3,684 report-image pairs, including 2,912 pairs for training and 772 pairs for testing. Different from existing methods [7, 8, 47, 48], we adopt both finding and impression sections as medical reports and remove the reports with less than 3 tokens for two datasets. There is no overlap of patients among different subsets. The CXR images with various sizes are all resized to  $256 \times 256$  pixels.

**Implementation Details** We adopt the PVT-medium [43] pre-trained with the disease classification task as the image encoder with AdaPatch in stage 2, 3 and 4. The AdaMatch is optimized with LAMB optimizer [51] and cosine learning rate scheduler [29]. The learning rate is 6e-3. The maximum training epoch is 15 and the per GPU batch size is 112. In AdaMatch-Cyclic, we adopt the VQ-GAN [13] models pre-trained on the MIMIC-CXR and OpenI datasets, respectively, and the dolly-v2-3b [9] model as pre-trained LLM. LLM has 5,1845 token types with 5,0821 token types for text tokens and 1,024 token types for image tokens. LLM is optimized by the AdamW [30] optimizer with a learning rate of 5e-6 and per GPU batch size of 24. The training epoch is 5. 8 Nvidia A100 40GB GPUs are used for all experiments. For more details, see supplementary materials.

**Evaluation Metrics** We evaluate the CXR-to-report generation performance with BLEU [33], METEOR [12], and ROUGE-L [27]. The FID [15] and NIQE [31] are utilized to evaluate report-to-CXR generation. The performance of CXR-to-report and report-to-CXR retrieval is assessed through the exact report in the top K retrieved reports for a given CXR image (R@K, K={1, 5, 10}).

### 4.2. Comparison with State-of-the-Arts.

#### 4.2.1 CXR-to-Report Generation

We verify the effectiveness of AdaMatch-Cyclic on the MIMIC-CXR and OpenI datasets for report generation. Since previous methods [7, 8, 39, 42, 47, 48] are mainly trained on the medical reports with the finding section, we reimplement previous methods on datasets with both finding and impression sections. In Table 1, our AdaMatch-Cyclic substantially surpasses the M2KT [47] by a significant margin with the BLEU-1 of 0.0132 in the MIMIC-CXR dataset. Moreover, we evaluate the OpenI dataset with



CXR Image	Ground-truth	M2KT	AdaMatch-Cyclic	Keywords
	PA and lateral views of the chest. Bilateral upper lobe <b>scarring</b> is seen with superior retraction of the hila. The lung volumes are relatively low. There is no evidence of superimposed acute process. Cardiomeastinal silhouette is stable. <b>Surgical clips in the upper abdomen again noted. Osseous structures are essentially unremarkable</b> noting probable right glenoid orthopedic hardware. Bilateral upper lobe <b>scarring</b> unchanged without evidence of superimposed acute process.	PA and lateral views of the chest were obtained. The patient is status post median sternotomy and cabg. The heart is normal in size. the mediastinal and hilar contours appear unchanged. There is no pleural effusion or pneumothorax. The pulmonary vasculature is not engorged. Patchy opacity in the right lower lung is concerning for pneumonia in the appropriate clinical setting. Patchy opacities in the right lung base may reflect atelectasis or pneumonia.	Heart size is mildly enlarged. Mediastinal and hilar contours are unremarkable. Pulmonary vasculature is normal. Mild elevation of the right hemidiaphragm is unchanged. <b>Scarring</b> within the left lung base is re-demonstrated with a left basilar calcified granuloma re-demonstrated. There is no focal consolidation pleural effusion or pneumothorax. <b>No acute osseous abnormality is visualized. Clips from prior cholecystectomy are noted in the right upper quadrant of the abdomen.</b> A percutaneous catheter is noted within the right upper quadrant of the abdomen. No evidence for pneumonia or congestive heart failure.	<b>upper lobe, bilateral, scarring,</b> thoracic vertebral body, edema, reticular opacities, semi-upright, <b>tube</b> side port, right pneumothorax
CXR Image	Ground-truth	R2GenCMN	AdaMatch-Cyclic	Keywords
	Small calcification right lung base with appearance of <b>old granulomatous disease</b> . Also small perihilar calcified lymph XXXX. Lungs are clear. No active parenchymal disease. No XXXX of pleural effusions. No pulmonary edema. Normal heart size. No XXXX of active cardiopulmonary disease. Unchanged.	Heart size is normal. The mediastinal and hilar contours are normal. The pulmonary vasculature is normal. Lungs are clear. No pleural effusion or pneumothorax is seen. There are no acute osseous abnormalities. No acute cardiopulmonary abnormality.	The trachea is midline. The heart is normal in size. The mediastinum is unremarkable. <b>Mild granulomatous sequela are noted.</b> The lungs are grossly clear. There is no pneumothorax. No acute disease.	lung, old, <b>calcification, lymph,</b> perihilar, airway, indwelling, <b>calcified granuloma,</b> hypoinflation, hiatal

Figure 5. Qualitative comparison with existing methods in CXR-to-report generation on the MIMIC-CXR (1st row) and OpenI datasets (2nd row). The texts in different colors show similar meanings. The keywords on the right are obtained from AdaMatch model.

Table 1. CXR-to-report generation performance in comparison to existing methods on MIMIC-CXR and OpenI datasets.

Methods	MIMIC-CXR						OpenI					
	BLEU-1	BLEU-2	BLEU-3	BLEU-4	METEOR	ROUGE-L	BLEU-1	BLEU-2	BLEU-3	BLEU-4	METEOR	ROUGE-L
R2Gen [7] (2020)	0.3553	0.2232	0.1523	0.1038	0.1412	0.2784	0.3992	0.2407	0.1518	0.0973	0.1390	0.3052
R2GenCMN [8] (2021)	0.3719	0.2332	0.1538	0.1053	0.1501	0.2827	0.4091	0.2493	0.1594	0.1045	0.1509	0.3181
Yang <i>et al.</i> [48] (2021)	0.3585	0.2266	0.1550	0.1021	0.1425	0.2788	0.3833	0.2409	0.1598	0.1078	0.1457	0.3293
XProNet [42] (2022)	0.3532	0.2212	0.1498	0.1052	0.1415	0.2811	0.4114	0.2502	0.1598	0.1045	0.1457	0.3240
ITHN [39] (2023)	0.3623	0.2128	0.1402	0.0992	0.1488	0.2622	0.2661	0.1516	0.0976	0.0663	0.1561	0.2617
M2KT [47] (2023)	0.3661	0.2192	0.1465	0.1044	0.1528	0.2673	0.2559	0.1381	0.0819	0.0523	0.1468	0.2439
AdaMatch-Cyclic	<b>0.3793</b>	<b>0.2346</b>	<b>0.1540</b>	<b>0.1060</b>	<b>0.1625</b>	<b>0.2859</b>	<b>0.4161</b>	<b>0.3002</b>	<b>0.2073</b>	<b>0.1446</b>	<b>0.1621</b>	<b>0.3656</b>

the model trained on the MIMIC-CXR dataset. In terms of the zero-shot report generation, our AdaMatch-Cyclic achieves the best performance with the BLEU-1, METEOR, ROUGE-L of 0.4161, 0.1621, and 0.3656. To further compare with GPT-4V[49], we randomly select 50 cases from the test set of the MIMIC-CXR dataset. In Table 2, our AdaMatch-Cyclic significantly outperforms the GPT-4V by 0.1479 and 0.0892 of BLEU-1 and BLEU-4, indicating our superiority to existing methods.

To qualitatively evaluate report generation performance, we show two cases of generated reports in Fig. 5. In comparison to M2KT [47] and R2GenCMN [8], our AdaMatch-Cyclic can obtain the related keywords (e.g. scarring and atelectasis) and correctly describes the ‘osseous abnormality’ and ‘clips in the right upper quadrant of the abdomen’ in the first case, and point out ‘mild granulomatous’ in the second case, suggesting that our method can generate medical reports with higher quality than previous methods.

Table 2. CXR-to-report generation performance in comparison to GPT-4V on 50 selected cases of the MIMIC-CXR dataset.

Methods	BLEU-1	BLEU-2	BLEU-3	BLEU-4
R2Gen[7](2020)	0.3513	0.2174	0.1447	0.1025
R2GenCMN[8](2021)	0.3587	0.2200	0.1436	0.0969
Yang <i>et al.</i> [48](2021)	0.3596	0.2218	0.1481	0.1026
XProNet[42](2022)	0.3356	0.2071	0.1374	0.0941
ITHN[39](2023)	0.3301	0.1839	0.1121	0.0723
M2KT[47](2023)	0.3626	0.2123	0.1391	0.0957
GPT-4V[49](2023)	0.2275	0.0878	0.0378	0.0166
AdaMatch-Cyclic	<b>0.3754</b>	<b>0.2303</b>	<b>0.1520</b>	<b>0.1058</b>

#### 4.2.2 Report-to-CXR Generation

To quantitatively assess the performance, we compare our method with the text-to-image generation method [37] and some report-to-CXR generation methods [2, 3, 22, 23]. As

Table 3. Report-to-CXR generation performance in comparison to existing methods on MIMIC-CXR and OpenI datasets.

Methods	MIMIC-CXR		OpenI	
	FID↓	NIQE↓	FID↓	NIQE↓
Stable diffusion [37]	9.2334	3.7894	8.2946	6.3496
Chambon <i>et al.</i> [3]	8.2758	3.8871	5.8557	4.6534
RoentGen [2]	9.5411	3.8834	6.5675	4.9085
UniXGen [22]	6.7212	3.7125	11.9890	4.6610
LLM-CXR [23]	2.1788	3.5969	1.6597	3.8206
AdaMatch-Cyclic	<b>1.0916</b>	<b>3.3931</b>	<b>1.5938</b>	<b>3.3096</b>

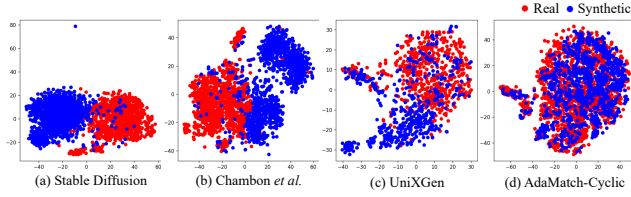


Figure 6. The t-SNE visualization of the real and synthetic CXR images on the MIMIC-CXR dataset.

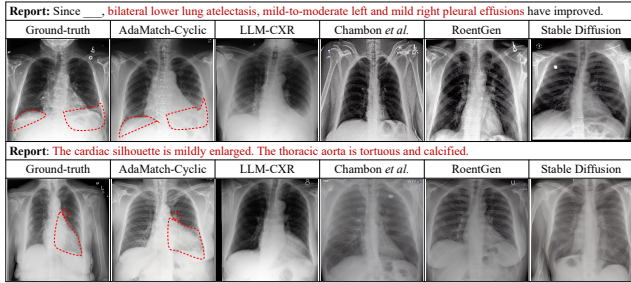


Figure 7. The generated chest X-ray images of the MIMIC-CXR (1st row) and OpenI (2nd row) datasets with highlighted regions.

listed in Table 3, AdaMatch-Cyclic achieves the best performance with 1.0916 and 1.5938 of FID scores on the MIMIC-CXR and OpenI datasets, respectively, indicating the superiority of our method over previous methods. To compare the high-level feature distribution of CXR images generated by different methods, we randomly select 1,000 cases from the test set, and apply the t-SNE visualization to the real and synthetic CXR images on the MIMIC-CXR dataset. As depicted in Fig. 6, synthetic CXR images generated by existing methods and real ones differ significantly from each other, while CXR images synthesized by AdaMatch-Cyclic almost overlap with the real CXR images. It implies that AdaMatch-Cyclic is more effective in translating medical reports to realistic CXR images compared to existing methods.

In Fig. 7, we show the generated CXR images of the MIMIC-CXR and OpenI datasets. In the first example, our

Table 4. CXR-report retrieval performance (%) in comparison to existing methods on the MIMIC-CXR dataset.

Methods	CXR-to-Report			Report-to-CXR		
	R@1	R@5	R@10	R@1	R@5	R@10
Fang <i>et al.</i> [14] (2015)	18.60	43.10	56.10	18.13	43.20	55.97
Chauhan <i>et al.</i> [4] (2020)	5.37	19.43	30.73	5.40	20.23	30.23
ConVIRT [53] (2020)	30.10	53.90	63.80	29.20	54.70	64.40
GLoRIA [16] (2021)	30.30	57.50	66.50	24.00	51.80	62.80
JoImTeR-Net [18] (2021)	18.93	46.20	58.67	19.07	45.27	58.50
MGCA [41] (2022)	25.80	51.90	62.10	27.90	51.20	61.60
LIMITR [10] (2023)	39.70	63.20	71.70	37.70	62.10	71.30
Motor [26] (2023)	10.96	31.93	42.90	12.00	33.10	44.32
AdaMatch	<b>51.47</b>	<b>86.19</b>	<b>94.77</b>	<b>51.18</b>	<b>86.46</b>	<b>94.60</b>

Table 5. Ablation study on AdaMatch w/o AdaPatch.

AdaPatch	CXR-to-Report			Report-to-CXR		
	R@1	R@5	R@10	R@1	R@5	R@10
✗	48.77	83.89	92.94	48.72	83.95	92.90
✓	<b>51.47</b>	<b>86.19</b>	<b>94.77</b>	<b>51.18</b>	<b>86.46</b>	<b>94.60</b>

AdaMatch-Cyclic can synthesize the ‘left and right pleural effusions’ as highlighted in the CXR images, while other methods [2, 3, 37] cannot generate the CXR images with ‘pleural effusions’. It suggests that our method can generate more realistic CXR images than existing methods according to the input report.

### 4.2.3 CXR-Report Retrieval

To prove the superiority of AdaMatch, we evaluate the CXR-to-report and report-to-CXR retrieval performance on the MIMIC-CXR datasets in comparison with existing methods. As listed in Table 4, our AdaMatch achieves the best retrieval performance, surpassing the LIMITR [10] by a large margin with R@1 of 11.77% and 13.48% for CXR-to-report and report-to-CXR retrieval, respectively, implying that our method is more effective in extracting distinct semantic features for CXR images and medical reports and is able to align their features correctly.

### 4.3. Ablation Study

**Effectiveness of AdaPatch.** To prove the effectiveness of AdaPatch, we compare the CXR-report retrieval performance of AdaMatch model with or without AdaPatch. In the AdaMatch model without AdaPatch, we use PVT-medium [43] as the image encoder. In Table 5, the AdaPatch module remarkably improves the R@1 by 2.70% and 2.46% for CXR-to-report and report-to-CXR retrieval, respectively, indicating the effectiveness of our AdaPatch.



Table 6. CXR-report retrieval performance of AdaMatch with different stages.

Stage	CXR-to-Report			Report-to-CXR		
	R@1	R@5	R@10	R@1	R@5	R@10
2	42.28	78.75	89.85	42.81	78.96	89.67
3	<b>51.47</b>	<b>86.19</b>	<b>94.77</b>	<b>51.18</b>	<b>86.46</b>	<b>94.60</b>
4	49.68	83.04	92.67	49.39	83.09	92.84

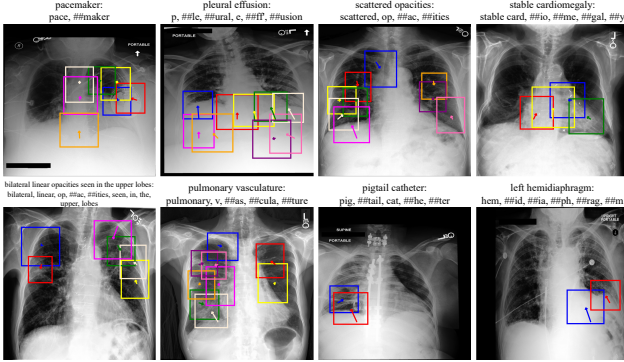


Figure 8. Visualization of texts and the corresponding adaptive patches. The boxes and arrows in different colors show adaptive patches and their shift of center from fixed patches.

**Image Encoder with Different Stages.** In AdaMatch, the image encoder consists of four stages, and the stage 2,3 and 4 include an AdaPatch module, respectively. To investigate the effectiveness of each stage for CXR-report alignment, we use patch embeddings from different stages to compute the CXR-report similarity for CXR-report retrieval task. In Table 6, the image encoder with three stages achieves the best retrieval performance with the R@1 of 51.47%, implying that the features of the 3rd stage are more beneficial for patch-word matching.

**Visualization of Adaptive Patches.** To visualize adaptive patches in AdaPatch, we display several examples from the MIMIC-CXR datasets. In Fig. 8, each example includes the text, its text tokens, and the corresponding CXR image with the marked adaptive patches. The adaptive patches are marked by the bounding boxes with different colors. Each bounding box includes an arrow, which shows the shift of center from the fixed patch to the adaptive patch. In the first example, adaptive patches cover the pacemaker and its wire. Meanwhile, adaptive patches of the second example show the correct position of pleural effusions in the CXR image. These indicate that AdaPatch can correctly localize the region relevant to input text tokens.

## 5. Conclusion

We propose an AdaMatch for fine-grained image-text alignment, which presents the first work to adaptively associate image patches with words and improve the

explainability of cyclic CXR-report generation. It includes the AdaPatch to acquire adaptive patches for abnormal regions, and performs patch-word alignment between adaptive patches with textual tokens. We implement cyclic CXR-report generation by using AdaMatch to provide explanations for the generation process. In addition, the fine-grained cyclic generation process supplies a natural explainability for the alignment between medical images and reports. Extensive experiments on two publicly available CXR datasets prove the effectiveness of our method and its superiority over previous methods.

## References

- [1] Emily Alsentzer, John Murphy, William Boag, Wei-Hung Weng, Di Jindi, Tristan Naumann, and Matthew McDermott. Publicly available clinical bert embeddings. pages 72–78, 2019. 4
- [2] Pierre Chambon, Christian Bluethgen, Jean-Benoit Delbrouck, Rogier Van der Sluijs, Małgorzata Polacin, Juan Manuel Zambrano Chaves, Tanishq Mathew Abraham, Shivanshu Purohit, Curtis P Langlotz, and Akshay Chaudhari. Roentgen: vision-language foundation model for chest x-ray generation. *arXiv preprint arXiv:2211.12737*, 2022. 3, 7, 8
- [3] Pierre Chambon, Christian Bluethgen, Curtis P Langlotz, and Akshay Chaudhari. Adapting pretrained vision-language foundational models to medical imaging domains. *arXiv preprint arXiv:2210.04133*, 2022. 3, 7, 8
- [4] Geeticka Chauhan, Ruizhi Liao, William Wells, Jacob Andreas, Xin Wang, Seth Berkowitz, Steven Horng, Peter Szolovits, and Polina Golland. Joint modeling of chest radiographs and radiology reports for pulmonary edema assessment. In *MICCAI*, pages 529–539. Springer, 2020. 8
- [5] Xiaofei Chen, Yuting He, Cheng Xue, Rongjun Ge, Shuo Li, and Guanyu Yang. Knowledge boosting: Rethinking medical contrastive vision-language pre-training. In *MICCAI*, pages 405–415. Springer, 2023. 2
- [6] Yen-Chun Chen, Linjie Li, Licheng Yu, Ahmed El Kholy, Faisal Ahmed, Zhe Gan, Yu Cheng, and Jingjing Liu. Uniter: Universal image-text representation learning. In *ECCV*, pages 104–120. Springer, 2020. 1, 2, 4
- [7] Zhihong Chen, Yan Song, Tsung-Hui Chang, and Xiang Wan. Generating radiology reports via memory-driven transformer. In *EMNLP*, pages 1439–1449, 2020. 3, 6, 7
- [8] Zhihong Chen, Yaling Shen, Yan Song, and Xiang Wan. Cross-modal memory networks for radiology report generation. In *ACL*, pages 5904–5914, 2021. 3, 6, 7
- [9] Mike Conover, Matt Hayes, Ankit Mathur, Jianwei Xie, Jun Wan, Sam Shah, Ali Ghodsi, Patrick Wendell, Matei Zaharia, and Reynold Xin. Free dolly: Introducing the world’s first truly open instruction-tuned llm, 2023. 5, 6
- [10] Gefen Dawidowicz, Elad Hirsch, and Ayellet Tal. Limitr: Leveraging local information for medical image-text representation. *arXiv preprint arXiv:2303.11755*, 2023. 8
- [11] Dina Demner-Fushman, Marc D Kohli, Marc B Rosenman, Sonya E Shooshan, Laritza Rodriguez, Sameer Antani, George R Thoma, and Clement J McDonald. Preparing a

- collection of radiology examinations for distribution and retrieval. *JAMIA*, 23(2):304–310, 2016. 6
- [12] Michael Denkowski and Alon Lavie. Meteor universal: Language specific translation evaluation for any target language. In *ACL*, pages 376–380, 2014. 6
- [13] Patrick Esser, Robin Rombach, and Bjorn Ommer. Taming transformers for high-resolution image synthesis. In *CVPR*, pages 12873–12883, 2021. 5, 6
- [14] Hao Fang, Saurabh Gupta, Forrest Iandola, Rupesh K Srivastava, Li Deng, Piotr Dollár, Jianfeng Gao, Xiaodong He, Margaret Mitchell, John C Platt, et al. From captions to visual concepts and back. In *CVPR*, pages 1473–1482, 2015. 8
- [15] Martin Heusel, Hubert Ramsauer, Thomas Unterthiner, Bernhard Nessler, and Sepp Hochreiter. Gans trained by a two time-scale update rule converge to a local nash equilibrium. *NeurIPS*, 30:6629–6640, 2017. 6
- [16] Shih-Cheng Huang, Liyue Shen, Matthew P Lungren, and Serena Yeung. Gloria: A multimodal global-local representation learning framework for label-efficient medical image recognition. In *ICCV*, pages 3942–3951, 2021. 2, 8
- [17] Jiho Jang, Chaerin Kong, Donghyeon Jeon, Seonhoon Kim, and Nojun Kwak. Unifying vision-language representation space with single-tower transformer. In *AAAI*, pages 980–988, 2023. 1
- [18] Zhanghexuan Ji, Mohammad Abuzar Shaikh, Dana Moukheiber, Sargur N Srihari, Yifan Peng, and Mingchen Gao. Improving joint learning of chest x-ray and radiology report by word region alignment. In *MLMI*, page 110–119. Springer, 2021. 1, 2, 8
- [19] Chao Jia, Yinfei Yang, Ye Xia, Yi-Ting Chen, Zarana Parekh, Hieu Pham, Quoc Le, Yun-Hsuan Sung, Zhen Li, and Tom Duerig. Scaling up visual and vision-language representation learning with noisy text supervision. In *ICML*, pages 4904–4916. PMLR, 2021. 1
- [20] Alistair EW Johnson, Tom J Pollard, Seth J Berkowitz, Nathaniel R Greenbaum, Matthew P Lungren, Chih-ying Deng, Roger G Mark, and Steven Horng. Mimic-cxr, a de-identified publicly available database of chest radiographs with free-text reports. *Scientific data*, 6(1):317, 2019. 6
- [21] Wonjae Kim, Bokyung Son, and Ildoo Kim. Vilt: Vision-and-language transformer without convolution or region supervision. In *ICML*, pages 5583–5594. PMLR, 2021. 1, 2, 4
- [22] Hyungyung Lee, Wonjae Kim, Jin-Hwa Kim, Tackeun Kim, Jihang Kim, Leonard Sunwoo, and Edward Choi. Unified chest x-ray and radiology report generation model with multi-view chest x-rays. *arXiv preprint arXiv:2302.12172*, 2023. 3, 7, 8
- [23] Suhyeon Lee, Won Jun Kim, and Jong Chul Ye. Llm itself can read and generate cxr images. *arXiv preprint arXiv:2305.11490*, 2023. 3, 7, 8
- [24] Wei Li, Can Gao, Guocheng Niu, Xinyan Xiao, Hao Liu, Jiachen Liu, Hua Wu, and Haifeng Wang. Unimo: Towards unified-modal understanding and generation via cross-modal contrastive learning. *arXiv preprint arXiv:2012.15409*, 2020. 1, 2, 4
- [25] Xiujuan Li, Xi Yin, Chunyuan Li, Pengchuan Zhang, Xiaowei Hu, Lei Zhang, Lijuan Wang, Houdong Hu, Li Dong, Furu Wei, et al. Oscar: Object-semantics aligned pre-training for vision-language tasks. In *ECCV*, pages 121–137. Springer, 2020. 1, 2, 4
- [26] Bingqian Lin, Zicong Chen, Mingjie Li, Haokun Lin, Hang Xu, Yi Zhu, Jianzhuang Liu, Wenjia Cai, Lei Yang, Shen Zhao, et al. Towards medical artificial general intelligence via knowledge-enhanced multimodal pretraining. *arXiv preprint arXiv:2304.14204*, 2023. 8
- [27] Chin-Yew Lin. Rouge: A package for automatic evaluation of summaries. In *ACL*, pages 74–81, 2004. 6
- [28] Che Liu, Sibor Cheng, Miaojing Shi, Anand Shah, Wenjia Bai, and Rossella Arcucci. Imitate: Clinical prior guided hierarchical vision-language pre-training. *arXiv preprint arXiv:2310.07355*, 2023. 2
- [29] Ilya Loshchilov and Frank Hutter. Sgdr: Stochastic gradient descent with warm restarts. In *ICLR*, 2016. 6
- [30] Ilya Loshchilov and Frank Hutter. Decoupled weight decay regularization. In *ICLR*, 2018. 6
- [31] Anish Mittal, Rajiv Soundararajan, and Alan C Bovik. Making a “completely blind” image quality analyzer. *IEEE Signal Process. Lett.*, 20(3):209–212, 2012. 6
- [32] Jong Hak Moon, Hyungyung Lee, Woncheol Shin, Young-Hak Kim, and Edward Choi. Multi-modal understanding and generation for medical images and text via vision-language pre-training. *IEEE J. Biomed. Health Inform.*, 26(12):6070–6080, 2022. 2
- [33] Kishore Papineni, Salim Roukos, Todd Ward, and Wei-Jing Zhu. Bleu: a method for automatic evaluation of machine translation. In *ACL*, pages 311–318, 2002. 6
- [34] Alec Radford, Jong Wook Kim, Chris Hallacy, Aditya Ramesh, Gabriel Goh, Sandhini Agarwal, Girish Sastry, Amanda Askell, Pamela Mishkin, Jack Clark, et al. Learning transferable visual models from natural language supervision. In *ICML*, pages 8748–8763. PMLR, 2021. 1
- [35] Shaina Raza, Deepak John Reji, Femi Shajan, and Syed Raza Bashir. Large-scale application of named entity recognition to biomedicine and epidemiology. *PLOS Digit. Health*, 1(12):1–18, 2022. 5
- [36] Shaoqing Ren, Kaiming He, Ross Girshick, and Jian Sun. Faster r-cnn: Towards real-time object detection with region proposal networks. *NeurIPS*, 28, 2015. 2
- [37] Robin Rombach, Andreas Blattmann, Dominik Lorenz, Patrick Esser, and Björn Ommer. High-resolution image synthesis with latent diffusion models. In *CVPR*, pages 10684–10695, 2022. 3, 7, 8
- [38] Ramprasaath R Selvaraju, Michael Cogswell, Abhishek Das, Ramakrishna Vedantam, Devi Parikh, and Dhruv Batra. Grad-cam: Visual explanations from deep networks via gradient-based localization. In *ICCV*, pages 618–626, 2017. 2
- [39] Bhanu Voutharoja, Lei Wang, and Luping Zhou. Automatic radiology report generation by learning with increasingly hard negatives. pages 2427–2434, 2023. 3, 6, 7
- [40] Zhongwei Wan, Che Liu, Mi Zhang, Jie Fu, Benyou Wang, Sibor Cheng, Lei Ma, César Quilodrán-Casas, and Rossella

- Arcucci. Med-unic: Unifying cross-lingual medical vision-language pre-training by diminishing bias. *arXiv preprint arXiv:2305.19894*, 2023. 2
- [41] Fuying Wang, Yuyin Zhou, Shujun Wang, Varut Vardhanabhuti, and Lequan Yu. Multi-granularity cross-modal alignment for generalized medical visual representation learning. *NeurIPS*, 35:33536–33549, 2022. 1, 2, 8
- [42] Jun Wang, Abhir Bhalerao, and Yulan He. Cross-modal prototype driven network for radiology report generation. In *ECCV*, pages 563–579. Springer, 2022. 3, 6, 7
- [43] Wenhai Wang, Enze Xie, Xiang Li, Deng-Ping Fan, Kaitao Song, Ding Liang, Tong Lu, Ping Luo, and Ling Shao. Pyramid vision transformer: A versatile backbone for dense prediction without convolutions. In *ICCV*, pages 568–578, 2021. 4, 6, 8
- [44] Wenhui Wang, Hangbo Bao, Li Dong, Johan Bjorck, Zhiliang Peng, Qiang Liu, Kriti Aggarwal, Owais Khan Mohammed, Saksham Singhal, Subhojit Som, et al. Image as a foreign language: Beit pretraining for vision and vision-language tasks. In *CVPR*, pages 19175–19186, 2023. 1
- [45] Bin Yan and Mingtao Pei. Clinical-bert: Vision-language pre-training for radiograph diagnosis and reports generation. In *AAAI*, pages 2982–2990, 2022. 2
- [46] Jinyu Yang, Jiali Duan, Son Tran, Yi Xu, Sampath Chanda, Liqun Chen, Belinda Zeng, Trishul Chilimbi, and Junzhou Huang. Vision-language pre-training with triple contrastive learning. In *CVPR*, pages 15671–15680, 2022. 1
- [47] Shuxin Yang, Xian Wu, Shen Ge, Zhuozhao Zheng, S Kevin Zhou, and Li Xiao. Radiology report generation with a learned knowledge base and multi-modal alignment. *Med. Image Anal.*, 86:102798, 2023. 3, 6, 7
- [48] Yan Yang, Jun Yu, Jian Zhang, Weidong Han, Hanliang Jiang, and Qingming Huang. Joint embedding of deep visual and semantic features for medical image report generation. *IEEE Trans. on Multimed.*, 2021. 3, 6, 7
- [49] Zhengyuan Yang, Linjie Li, Kevin Lin, Jianfeng Wang, Chung-Ching Lin, Zicheng Liu, and Lijuan Wang. The dawn of lmms: Preliminary explorations with gpt-4v (ision). *arXiv preprint arXiv:2309.17421*, 2023. 7
- [50] Lewei Yao, Runhui Huang, Lu Hou, Guansong Lu, Minzhe Niu, Hang Xu, Xiaodan Liang, Zhenguo Li, Xin Jiang, and Chunjing Xu. Filip: Fine-grained interactive language-image pre-training. *arXiv preprint arXiv:2111.07783*, 2021. 1, 2, 4
- [51] Yang You, Jing Li, Sashank Reddi, Jonathan Hseu, Sanjiv Kumar, Srinadh Bhojanapalli, Xiaodan Song, James Demmel, Kurt Keutzer, and Cho-Jui Hsieh. Large batch optimization for deep learning: Training bert in 76 minutes. In *ICLR*, 2019. 6
- [52] Xunlin Zhan, Yangxin Wu, Xiao Dong, Yunchao Wei, Minlong Lu, Yichi Zhang, Hang Xu, and Xiaodan Liang. Productlm: Towards weakly supervised instance-level product retrieval via cross-modal pretraining. In *CVPR*, pages 11782–11791, 2021. 1, 2, 4
- [53] Yuhao Zhang, Hang Jiang, Yasuhide Miura, Christopher D Manning, and Curtis P Langlotz. Contrastive learning of medical visual representations from paired images and text. In *MLHC*, pages 2–25. PMLR, 2022. 8